Supporting Information

Immortal Ring-Opening Polymerization of Lactides with Super High Monomer to Catalyst Ratios Initiated by Zirconium and Titanium Complexes Containing Multidentate Amino-bis(phenolate) Ligands

Baolong Wang, Huanqin Zhao, Liying Wang,* Junmin Sun, Yongfeng Zhang, Zhenzhu Cao

School of Chemical Engineering, Institute of Coal Conversion and Cyclic Economy, Inner Mongolia University of Technology
49 Aimin Road, Hohhot, 010051, China
E-mail: wangliying7704@163.com

Table S1. Crystallographic data for complex **2**.

Empirical formula	$C_{74}H_{116}N_4O_6Zr{\cdot}C_7H_8$
Formula weight	1341.07
Temperature/K	282(2) K
Crystal system	triclinic
Space group	P-1
a/Å	11.8670(6)
b/Å	16.2871(9)
c/Å	24.4789(14)
α/°	105.498(2)
β/°	90.376(2)
γ/°	102.180(2)
Volume/Å^3	4446.6(4)
Z	2
ρ_{calc}mg/mm^3	1.002
m/mm^{-1}	0.169
F(000)	1452
Crystal size/mm^3	0.2 × 0.1 × 0.1
Theta Min-Max [Deg]	2.8 to 25.0°
Index ranges	-14 ≤ h ≤ 14, -19 ≤ k ≤ 19, -29 ≤ l ≤ 29
Radiation/ Å	MoKa /0.71073
Tot., Uniq. Data, R(int)	15681, 15681, 0.043
Observed data [I > 2.0 sigma(I)]	13671
Nref, Npar	15681, 848
R, wR2, S	0.0495, 0.1426, 1.00
Max. and Av. Shift/Error	0.00, 0.00
Min. and Max. Resd. Dens. [e/Ang^3]	-0.43, 0.81

Table S2. Selected bond lengths (Å) and angles (°) for complex **2**.

Zr1-N1	2.401(2)	Zr1-O2	2.01175(17)
Zr1-N2	2.418(2)	Zr1-O3	2.0135(16)
Zr1-O1	2.0231(17)	Zr1-O4	2.0118(16)
Zr1-N1- C15	106.97(14)	N1-Zr1-N2	175.31(7)
Zr1-N1-C16	109.75(14)	O1-Zr1-N1	78.16(7)
Zr1-N1-C31	109.81(14)	O1-Zr1-N2	98.10(7)
Zr1-N2-C34	105.84(13)	O2-Zr1-N1	80.72(7)
Zr1-N2-C49	107.71(14)	O2-Zr1-N2	103.13(7)
Zr1-N2-C64	113.13(14)	O1-Zr1-O2	158.72(7)
Zr1-O1- C1	143.44(15)	O3-Zr1-N1	98.47(7)
Zr1-O2-C18	140.52(15)	O3-Zr1-N2	78.98(7)
Zr1-O3-C40	142.88(15)	O1-Zr1-O3	95.55(7)
Zr1-O4- C55	143.08(15)	O2-Zr1-O3	90.06(7)
Zr1-O1-C1	143.44(15)	O4-Zr1-N1	102.42(7)
Zr1-O2-C18	140.52(15)	O4-Zr1-N2	80.33(7)
		O1-Zr1-O4	90.84(7)
		O2-Zr1-O4	91.17(7)
		O3-Zr1-O4	159.00(7)

Table S3. Crystallographic data for complex **3**.

Empirical formula	$C_{74}H_{122}N_4O_{10}Ti_2$
Formula weight	1323.50
Temperature/K	173(2) K
Crystal system	triclinic
Space group	P-1
a/Å	13.4552(12)
b/Å	13.5618(12)
c/Å	25.287(2)
α/°	96.117(3)
β/°	103.136(3)
γ/°	91.355(3)
Volume/Å^3	4462.5(7)
Z	2
ρ_{calc}mg/mm^3	0.985
m/mm^{-1}	0.226
F(000)	1436
Crystal size/mm^3	0.2 × 0.2 × 0.1
Θ range for data collection	2.81 to 23.23°
Index ranges	-14 ≤ h ≤ 14, -14 ≤ k ≤ 15, -28 ≤ l ≤ 27
Radiation/Å	MoKa / 0.71073
Tot., Uniq. Data, R(int)	12688, 12688, 0.086
Observed data [I > 2.0 sigma(I)]	9810
Nref, Npar	12688, 830
R, wR2, S	0.0588, 0.1580, 1.02
Max. and Av. Shift/Error	0.00, 0.00
Min. and Max. Resd. Dens. [e/Ang^3]	-0.40, 0.49

Table S4. Selected bond lengths (Å) and angles (°) for complex **3**.

Ti1-N1	2.398(2)	Ti1-O3	1.917(2)
Ti1-O1	2.395(2)	Ti1-O4	1.907(2)
Ti1-O2	1.773(2)	Ti1-O10	1.788(2)
Ti2-N4	2.414(3)	Ti2-O8	1.774(2)
Ti2-O6	1.905(2)	Ti2-O9	1.800(2)
Ti2-O7	1.911(2)	Ti2-O5	2.366(2)
Ti1-O1-C55	118.9(2)	O1-Ti1-O2	174.25(9)
Ti1-O1-C56	121.29(17)	O1-Ti1-O3	81.74(8)
Ti1-O2-C4	165.0(2)	O1-Ti1-O4	81.60(8)
Ti1-O3-C7	132.65(18)	O1-Ti1-O10	82.55(10)
Ti1-O4-C12	141.58(18)	O1-Ti1-N1	81.35(8)
Ti1-O10-C1	158.2(3)	O2-Ti1-O3	97.47(10)
Ti1-N1-C9	110.02(16)	O2-Ti1-O4	97.55(10)
Ti1-N1-C10	110.25(16)	O2-Ti1-O10	103.21(11)
Ti1-N1-C22	108.99(17)	O2-Ti1-N1	92.90(9)
Ti2-O6-C27	138.02(19)	O3-Ti1-O4	157.27(9)
Ti2-O7-C41	140.2(2)	O3-Ti1-O10	96.59(10)
Ti2-O8-C58	168.8(2)	O3-Ti1-N1	82.18(8)
Ti2-O9-C61'	148.4(5)	O4-Ti1-O10	96.46(10)
Ti2-N4-C38	110.29(16)	O4-Ti1-N1	80.12(9)
Ti2-N4-C39	109.60(17)	O10-Ti1-N1	163.86(10)
Ti2-N4-C51	107.91(16)	O6-Ti2-O7	157.34(10)
		O6-Ti2-O8	97.57(11)
		O6-Ti2-O9	97.46(10)
		O6-Ti2-N4	80.95(9)
		O7-Ti2-O8	95.97(10)
		O7-Ti2-O9	97.28(10)
		O7-Ti2-N4	80.10(9)
		O8-Ti2-O9	102.39(11)
		O8-Ti2-N4	93.77(9)
		O9-Ti2-N4	163.83(10)

Table S5. Ring-Opening polymerization of lactide initiated by complexes **1**-**4**.

Run	Cat.	Monomer	T/°C	$[LA]_0/[Cat]_0/[BnOH]_0$	t/(h)	Conv. [a] (%)	$M_{n,\,calcd}$ (10^4) [b]	(10^4) M_n [c]	PDI[c]	TOF [d]	P_r [e]
1.	**1**	*L*-LA	140	800/1/0	1	45	2.60	0.74	1.13	360	-
2.	**1**	*L*-LA	140	800/1/0	2	68	3.92	0.86	1.15	272	-
3.	**1**	*L*-LA	140	800/1/0	3	83	4.79	0.92	1.24	221	-
4.	**1**	*L*-LA	140	1200/1/0	2.5	56	4.85	1.86	1.24	269	-
5.	**1**	*L*-LA	140	1200/1/0	3.5	71	6.14	2.52	1.24	243	-
6.	**1**	*L*-LA	140	1200/1/0	4.5	76	6.57	2.97	1.27	203	-
7.	**1**	*L*-LA	140	1200/1/0	5.5	80	6.92	3.11	1.19	175	-
8.	**1**	*L*-LA	140	1600/1/0	4	49	5.65	1.25	1.15	196	-
9.	**1**	*L*-LA	140	1600/1/0	6	70	8.07	1.43	1.11	187	-
10.	**1**	*L*-LA	140	1600/1/0	7	77	8.88	2.17	1.15	176	-
11.	**1**	*rac*-LA	160	150 000/1/0	70	56	605.35	5.61	1.24	1200	0.51
12.	**1**, [f]	*rac*-LA	160	1000/1/0	41	90	6.49	3.43	1.26	22	0.59
13.	**2**	*rac*-LA	140	1200/1/0	5	72	6.23	3.02	1.29	173	0.62
14.	**2**	*rac*-LA	160	200 000/1/0	46	57	817.62	2.86	1.28	2478	0.60
15.	**2**	*rac-LA*	160	150 000/1/10	11	48	103.77	4.05	1.58	6574	0.64
16.	**2**	*rac-LA*	160	200 000/1/10	11	34	98.00	1.04	1.27	6121	0.61
17.	**2**	*rac-LA*	160	200 000/1/100	46	52	14.99	1.05	1.36	2247	0.61
18.	**2**	*rac*-LA	160	154 900/1/0	20	48	535.82	2.76	1.48	3718	0.67
19.	**2**	*rac*-LA	160	15 500/1/0	11.5	63	70.37	2.44	1.45	849	0.65
20.	**2**	*rac*-LA	160	31 000/1/0	11.5	57	127.34	2.66	1.48	1537	0.71
21.	**2**	*rac*-LA	160	46 500/1/0	10.5	55	184.31	2.69	1.43	2436	0.66
22.	**2**	*rac*-LA	160	77 400/1/0	10.5	53	295.63	2.86	1.46	3907	0.67
23.	**2**	*L*-LA	160	46 500/1/0	26	74	247.98	1.03	1.36	1323	-
24.	**2**	*L*-LA	160	77 400/1/0	31	63	351.41	0.99	1.33	1573	-
25.	**2**	*L*-LA	160	154 900/1/0	31	65	725.59	1.02	1.27	3248	-
26.	**3**	*L*-LA	140	500/1/0	4	43	1.55	0.62	1.20	54	-
27.	**3**	*L*-LA	140	500/1/0	6	57	2.07	0.87	1.31	48	-
28.	**3**	*L*-LA	140	1000/1/0	35	90	6.49	1.82	1.29	26	-
29.	**4**	*L*-LA	140	500/1/0	6.5	67	2.42	1.31	1.46	52	-
30.	**4**	*L*-LA	140	500/1/0	7.5	71	2.57	1.37	1.28	47	-

[a] Determined by ^1H NMR spectroscopy. [b] $M_{n,calcd}$ = 1/2 × ($[LA]_0/[\mathbf{Cat}]_0$) × 144.13 × Conv.% g mol^{-1}; with the presence of BnOH, $M_{n,calcd}$ = ($[LA]_0/[\mathbf{Cat}]_0/[\mathbf{BnOH}]_0$) × 144.13 × Conv.% g mol^{-1}. [c] Determined by GPC analysis with polystyrene standards in THF with the correction factor of x 0.58. [d] TOFs were calculated as (mol of LA consumed)/(mol of catalyst × time of polymerization) h^{-1}. [e] P_r is the probability of a racemic linkage between two repetitive units calculated from homonuclear decoupled ^1H NMR spectrum. [f] Under air environment.

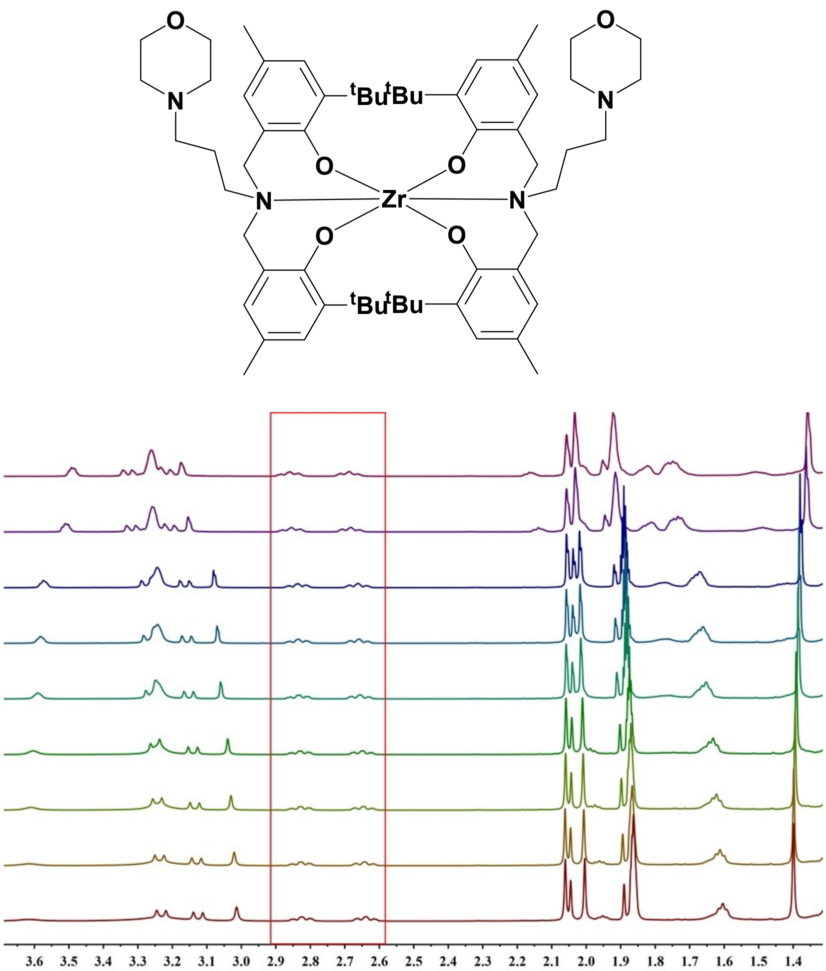

Figure S1 Variable-Temperature ^{1}H NMR spectra (500 MHz) of complex **1**.

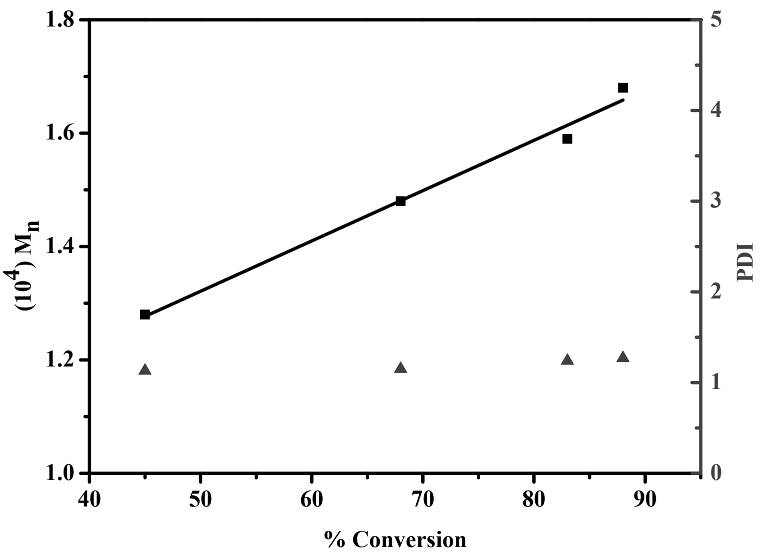

Figure S2 M_n and PDI *versus* conversion plots for ROP of *L*-latide initiated by complex **1**. (Condiction: $[LA]_0/[\mathbf{1}]_0$ = 800/1, R^2 = 0.9708; in the melt, at 140 ^oC.)

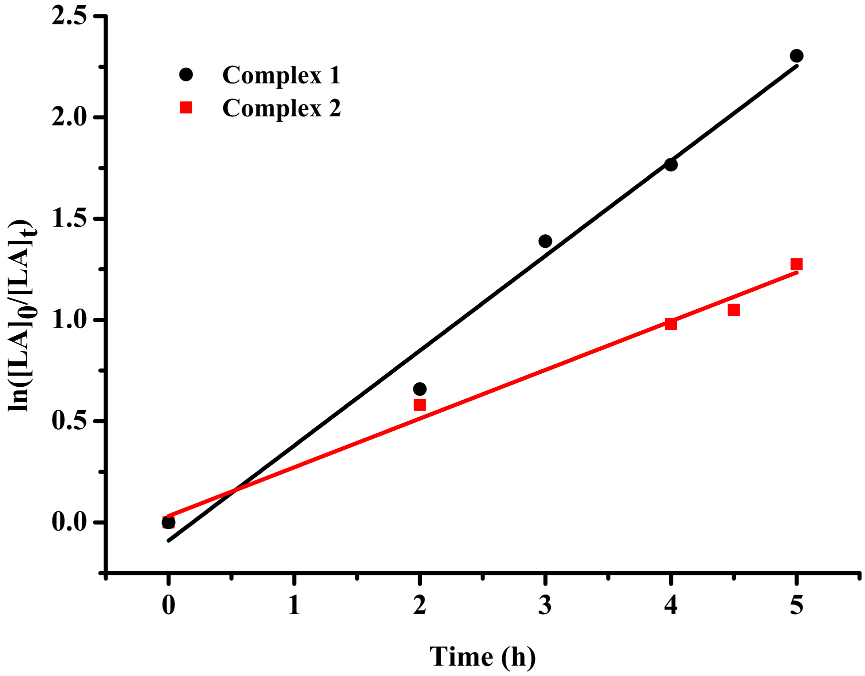

Figure S3 Plots of ln($[LA]_0/[LA]_t$) for ROP of *rac*-lactide *versus* time initiated by complexes **1** and **2**. (Conditions: $[LA]_0/[\mathbf{1}]_0$ = 1200/1, in the melt, at 140 °C, y = 0.4688x - 0.0894, R^2 = 0.9791; $[LA]_0/[\mathbf{2}]_0$ = 1200/1, in the melt, at 140 °C, y = 0.2406x + 0.0321, R^2 = 0.9846).

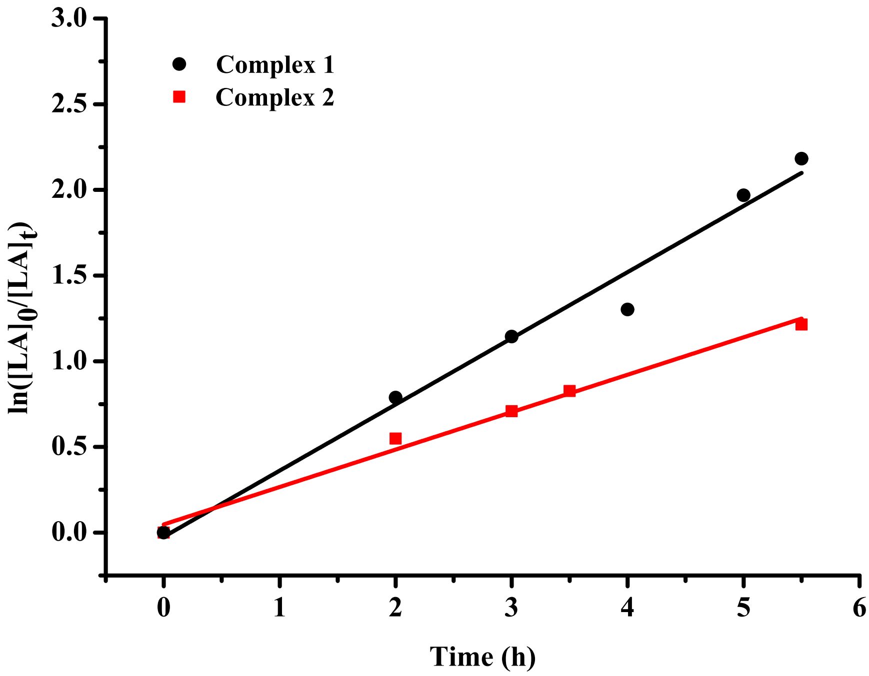

Figure S4 Plots of ln($[LA]_0/[LA]_t$) for ROP of *L*-lactide *versus* time initiated by complexes **1** and **2**. (Conditions: $[LA]_0/[\mathbf{1}]_0$ = 1000/1, in the melt, at 160 °C, y = 0.3861x – 0.0241, R^2 = 0.9761; $[LA]_0/[\mathbf{2}]_0$ = 1000/1, in the melt, at 160 °C, y = 0.2184x + 0.0481, R^2 = 0.9867).

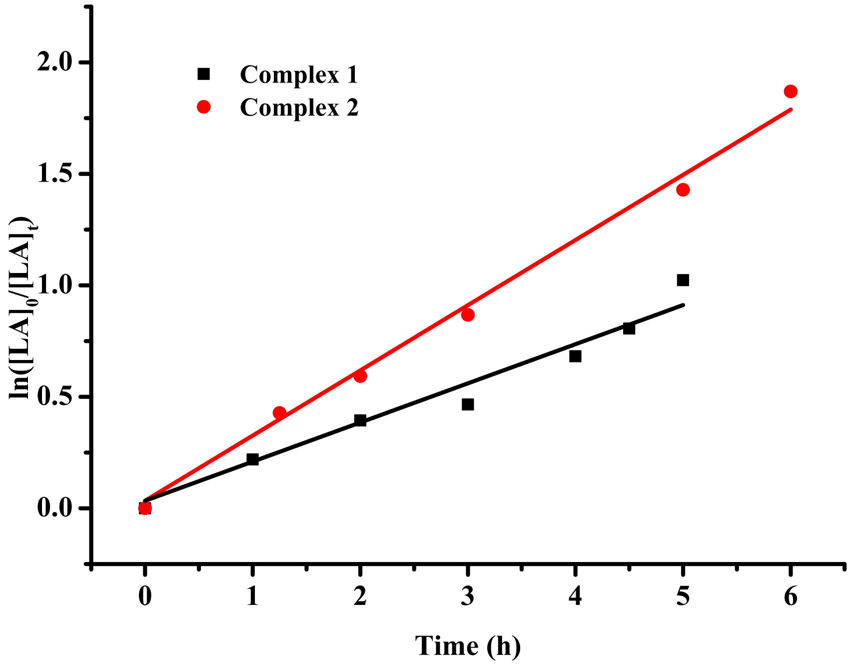

Figure S5 Plots of ln($[LA]_0/[LA]_t$) for ROP of *rac*-lactide *versus* time initiated by complexes **1** and **2**. (Conditions: $[LA]_0/[\mathbf{1}]_0$ = 1000/1, in the melt, at 160 ^oC, y = 0.1851x - 0.0031, R^2 = 0.9927; $[LA]_0/[\mathbf{2}]_0$ = 1000/1, in the melt, at 160 ^oC, y = 0.2993x + 0.0039, R^2 = 0.9622).

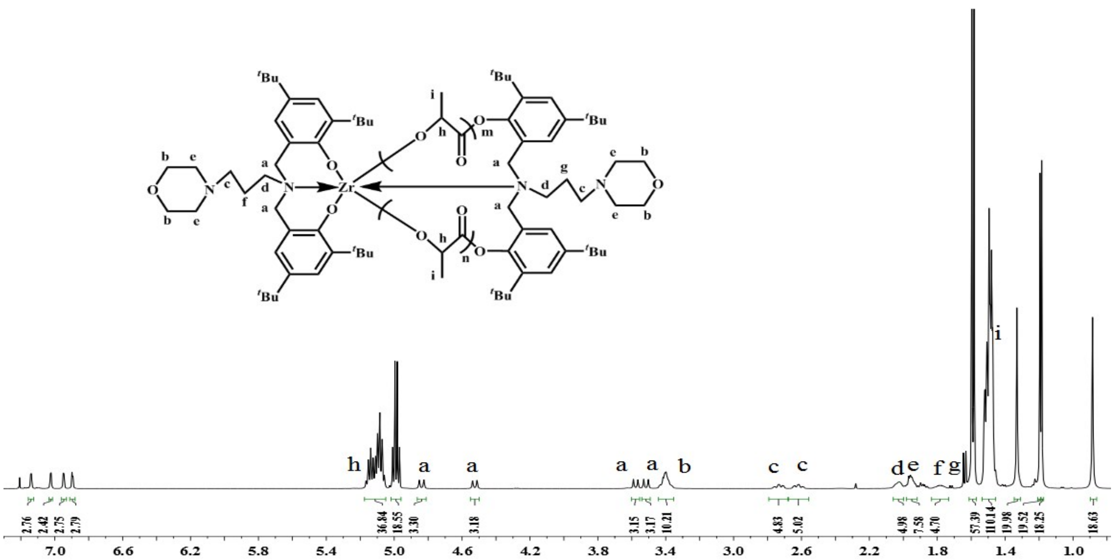

Figure S6 ^{1}H NMR spectra (500 MHz, $CDCl_3$) of the reaction of complex **2** with *rac*-lactide in the melt state. Conditions: $[LA]_0$: $[\mathbf{2}]_0$ = 20 : 1, 160 ^oC.

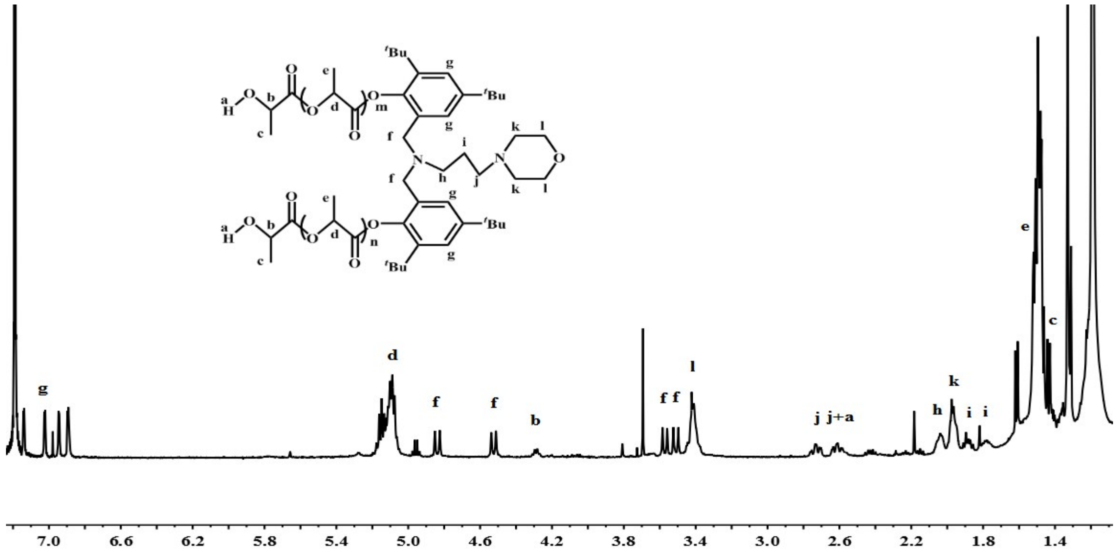

Figure S7 ^{1}H NMR spectra of oligomeric PLA obtained by complex **2** (500 MHz, $CDCl_3$). Conditions: $[LA]_0 : [\mathbf{2}]_0 = 50 : 1$, 160 °C.

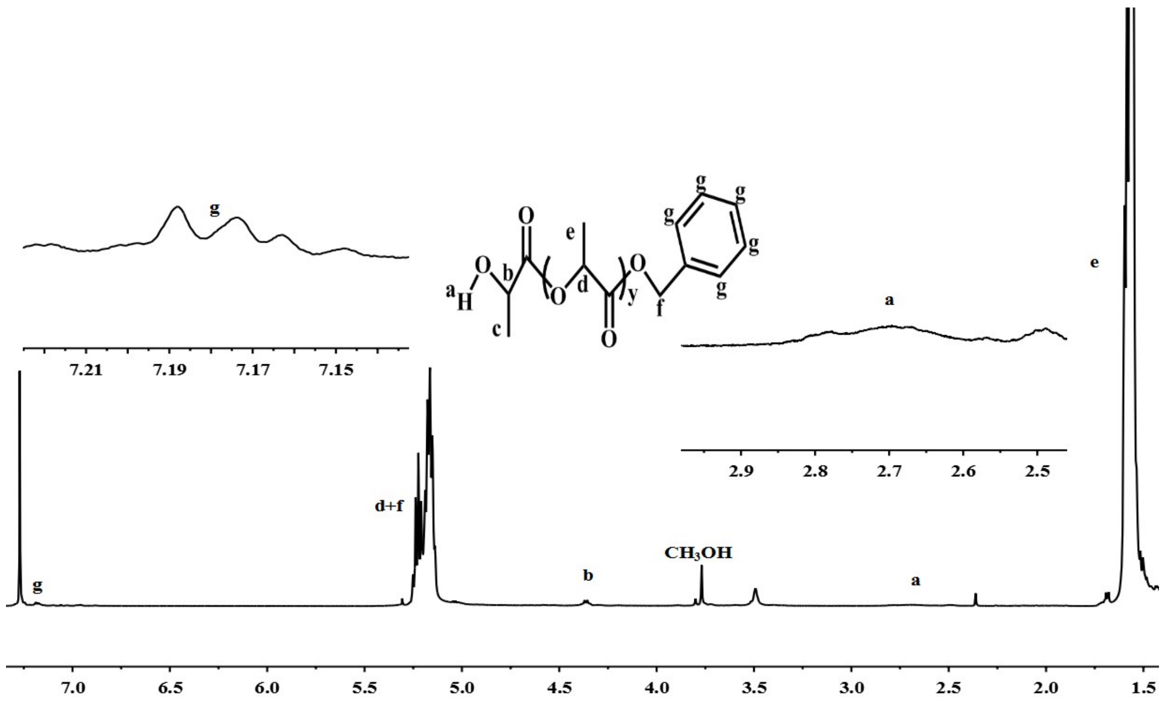

Figure S8 ^{1}H NMR spectra of oligomeric PLA obtained by complex **2** (500 MHz, $CDCl_3$). Conditions: $[LA]_0 : [\mathbf{2}]_0 : [BnOH]_0 = 50 : 1 : 1$, 160 °C.

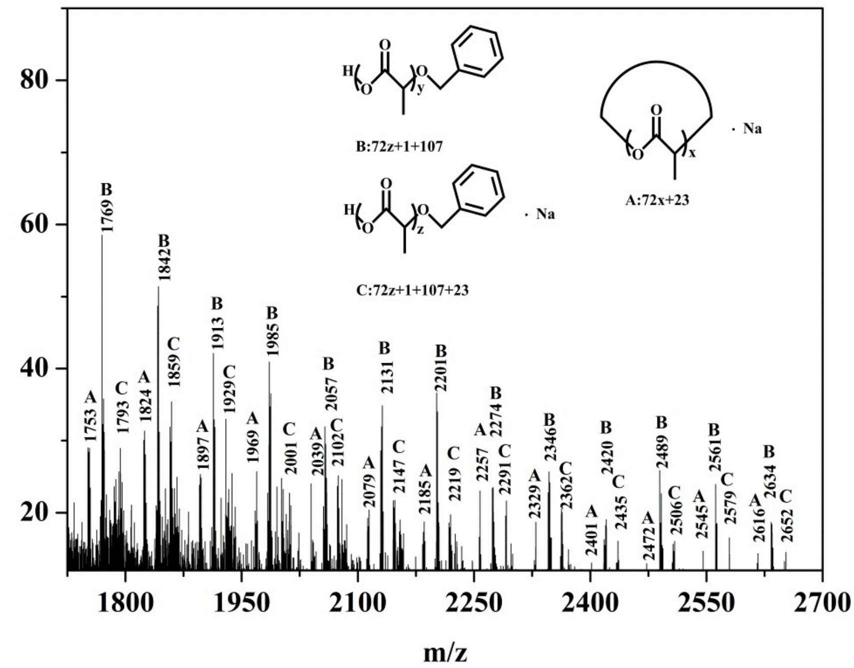

Figure S9 MALDI-TOF mass spectrum of the polymerization of *rac*-lactide initiated by complex **2**. Conditions: $[LA]_0$: $[\mathbf{2}]_0$: $[BnOH]_0$ = 1000 : 1 : 10, at 160 °C.

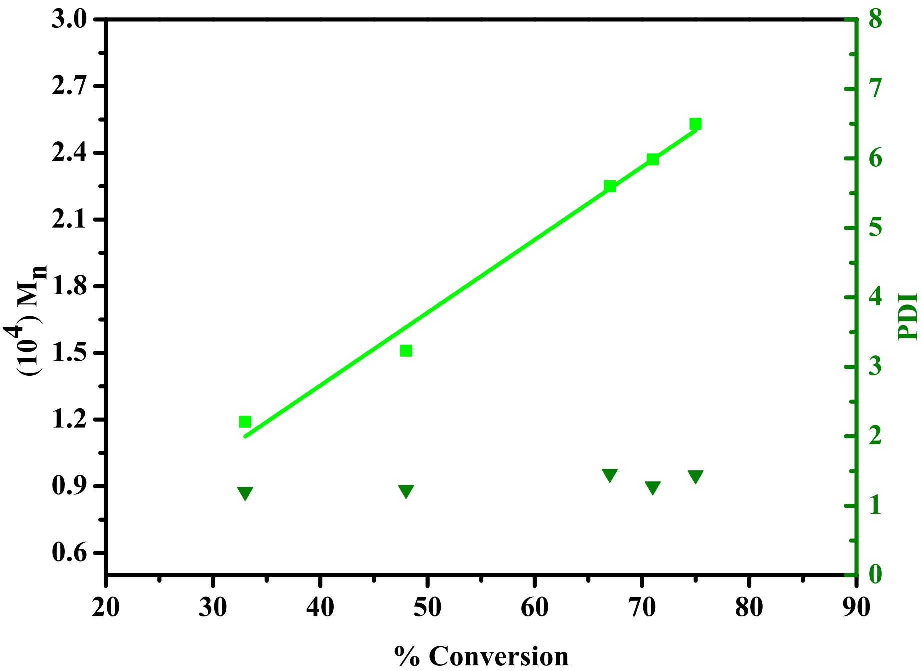

Figure S10 M_n and PDI *versus* conversion plots for ROP of *L*-latide initiated by complex **4**. (Condiction: $[LA]_0/[\mathbf{4}]_0$ = 500/1, at 140 °C, in the melt, R^2 = 0.9840)

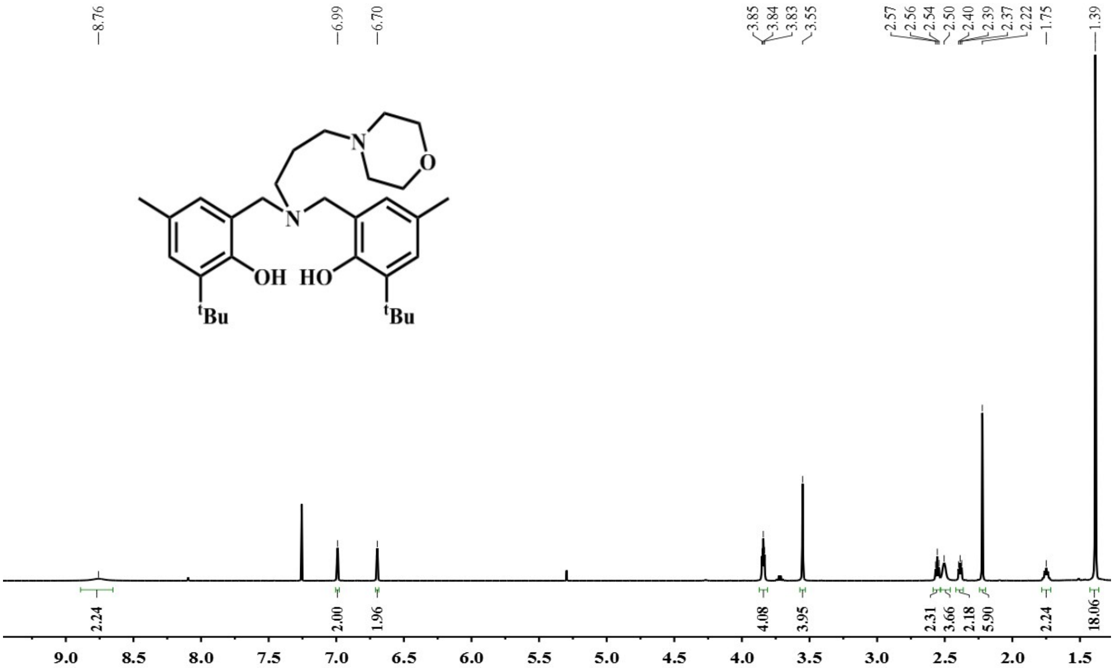

Figure S11 The ^{1}H NMR spectrum of ligand $L^{1}H$ ($CDCl_3$, 500MHz).

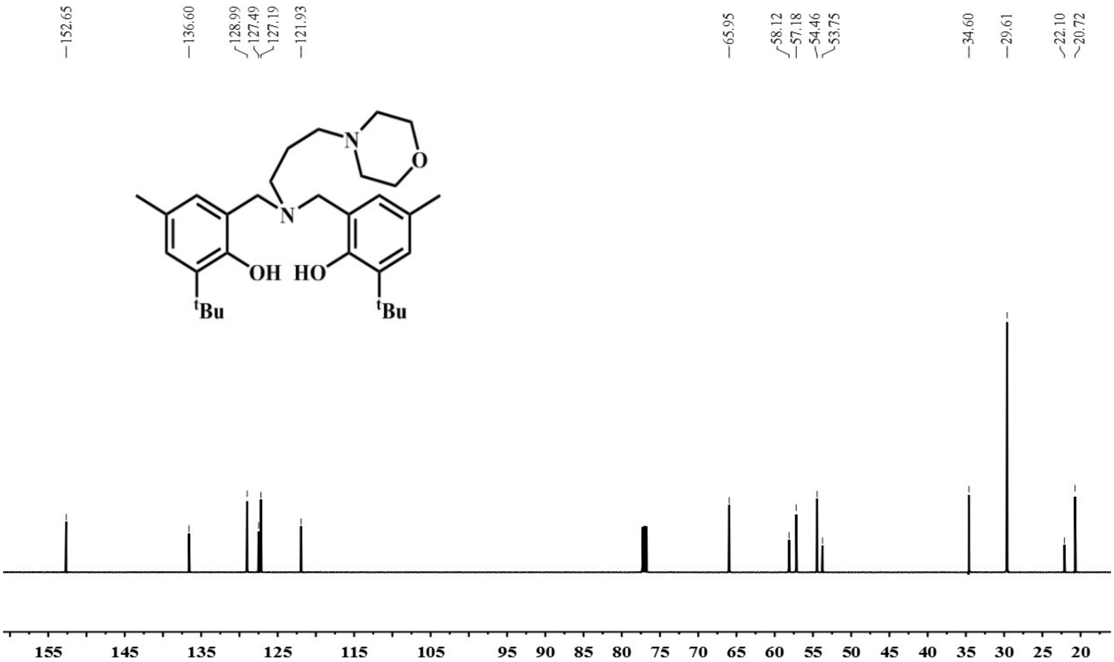

Figure S12 The ^{13}C NMR spectrum of ligand $L^{1}H$ ($CDCl_3$, 125MHz).

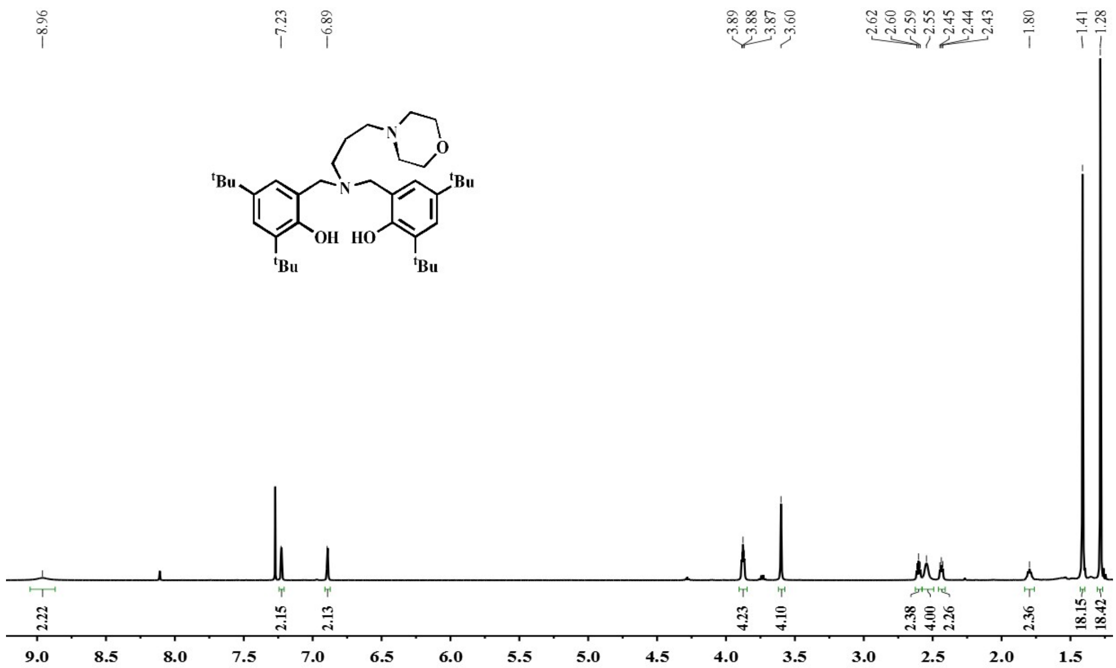

Figure S13 The ^{1}H NMR spectrum of ligand $L^{2}H$ ($CDCl_3$, 500MHz).

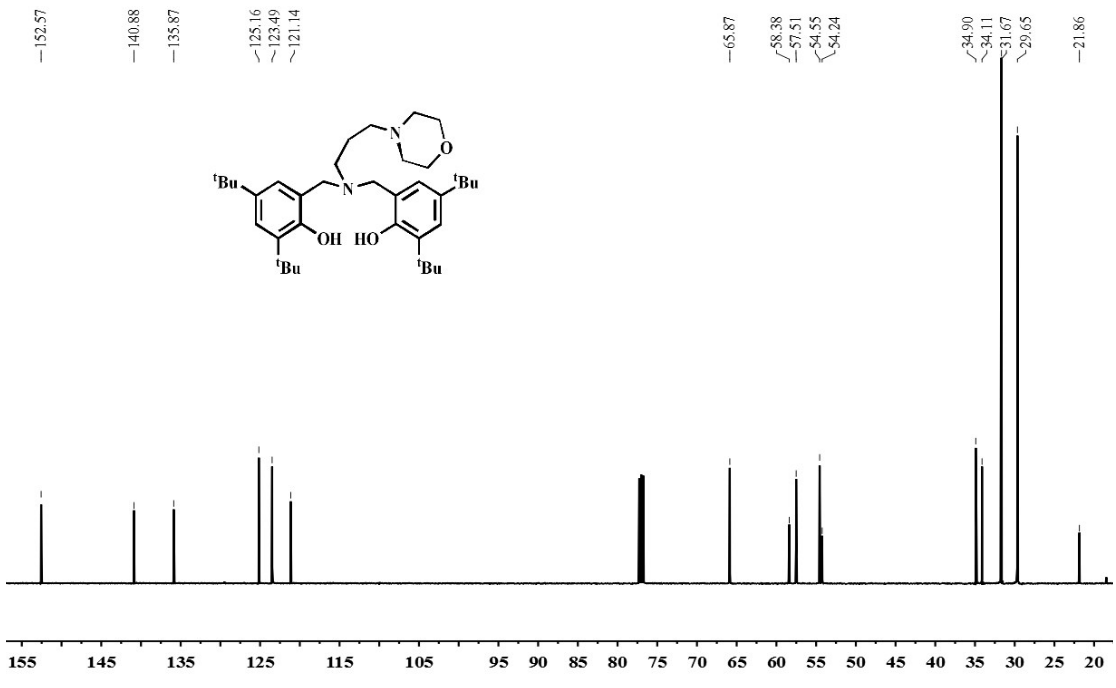

Figure S14 The ^{13}C NMR spectrum of ligand $L^{2}H$ ($CDCl_3$, 125MHz).

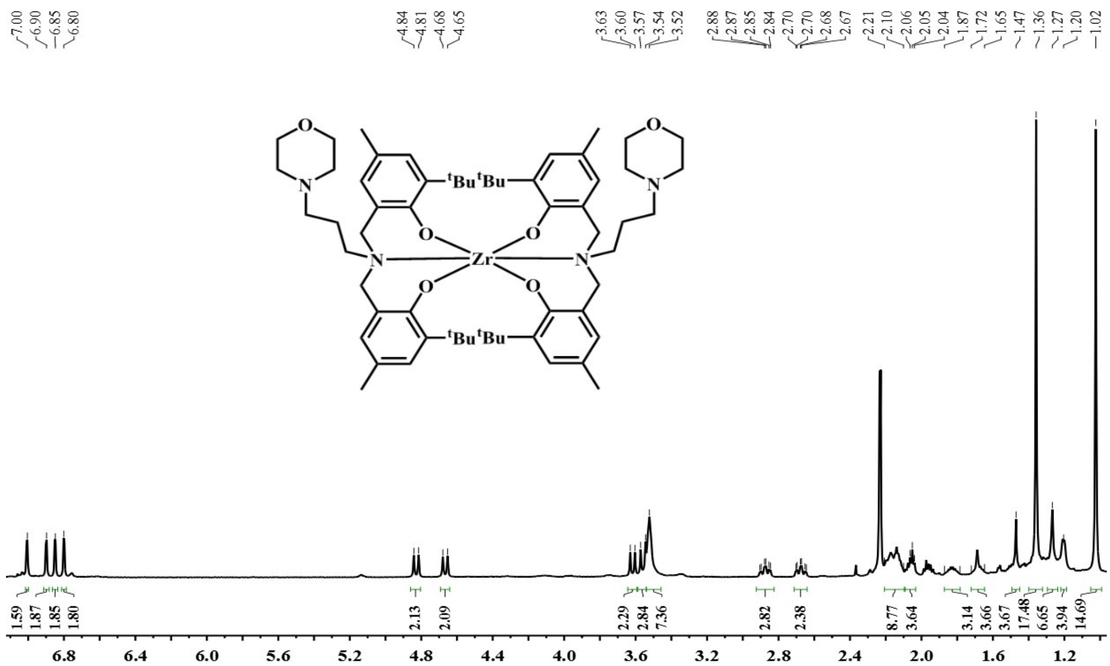

Figure S15 The [1]H NMR spectrum of complex **1** ($CDCl_3$, 500MHz).

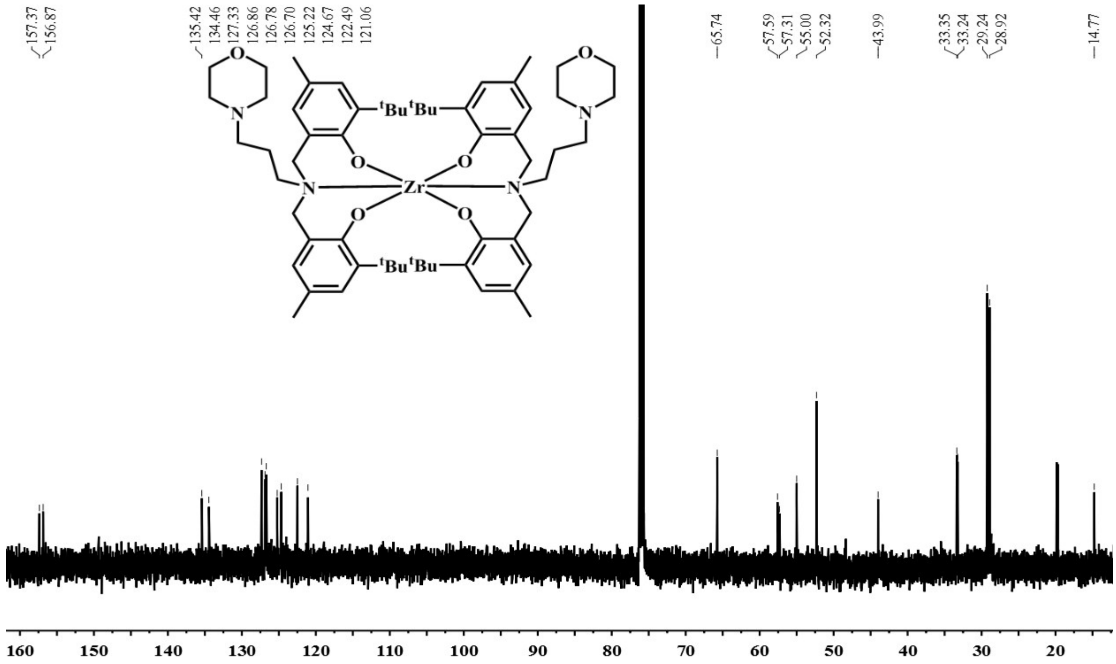

Figure S16 The [13]C NMR spectrum of complex **1** ($CDCl_3$, 125MHz).

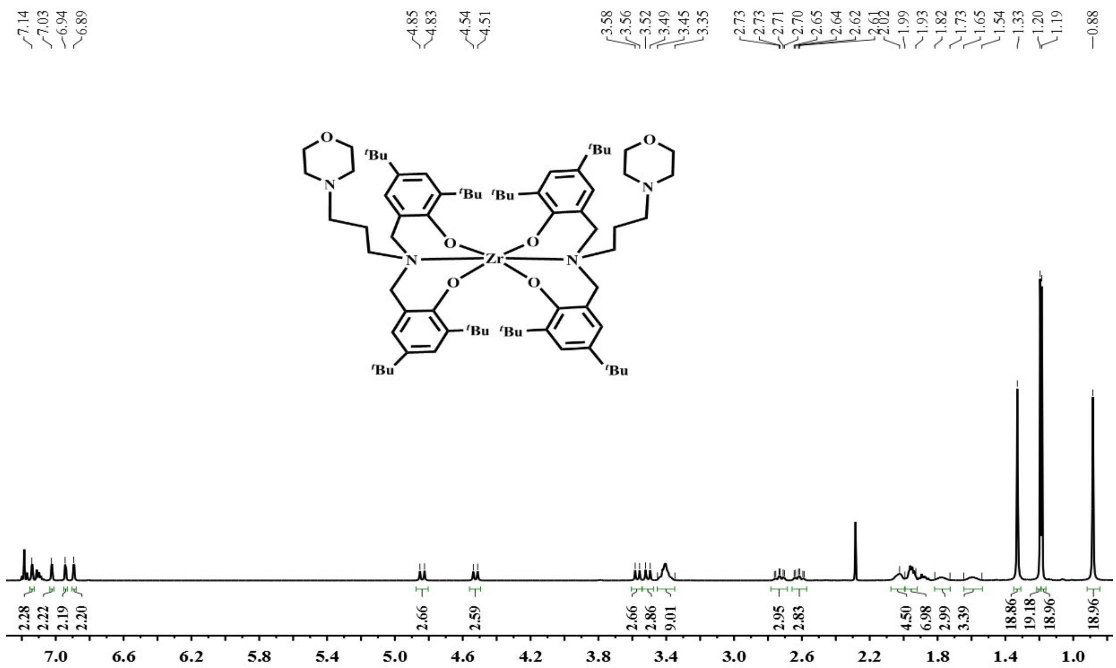

Figure S17 The ^{1}H NMR spectrum of complex **2** ($CDCl_3$, 500MHz).

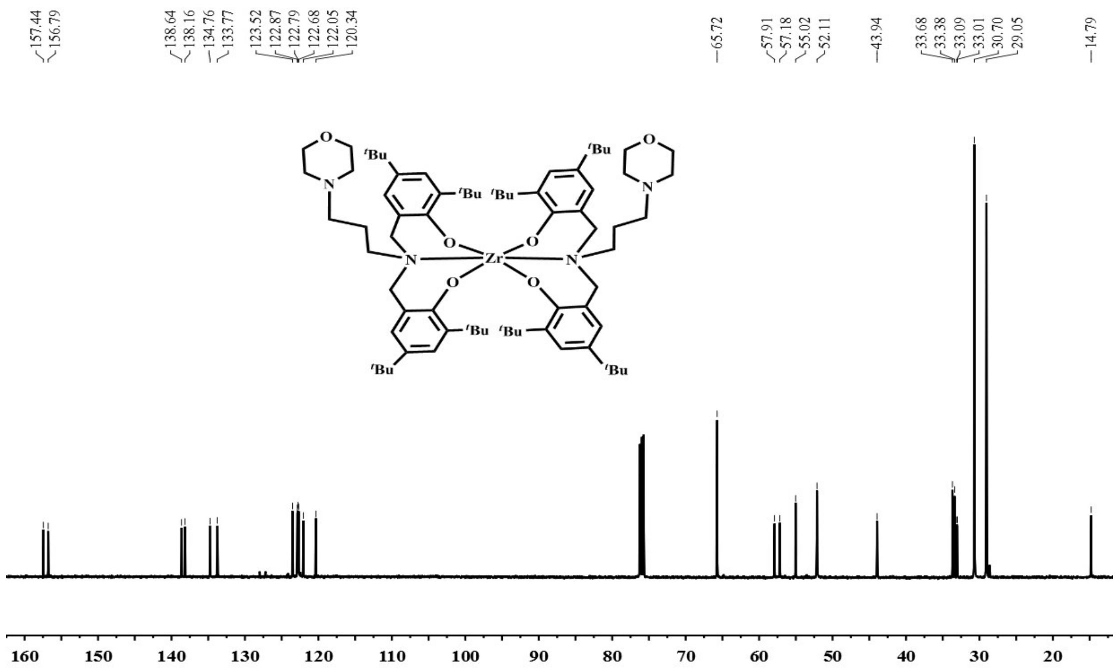

Figure S18 The ^{13}C NMR spectrum of complex **2** ($CDCl_3$, 125MHz).

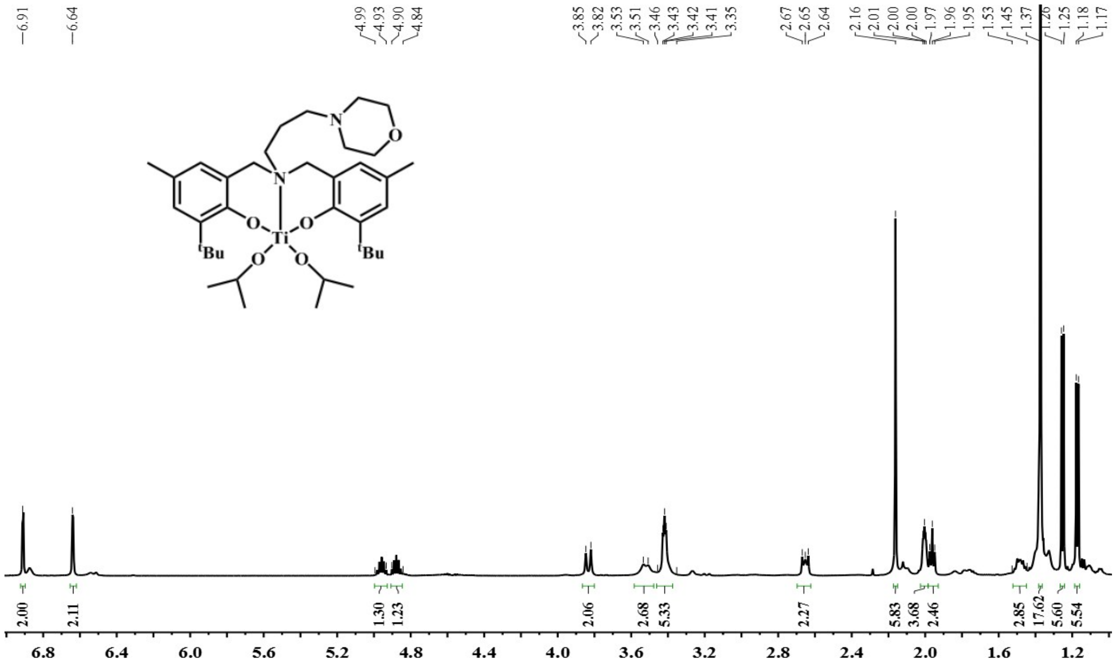

Figure S19 The ^{1}H NMR spectrum of complex **3** ($CDCl_3$, 500MHz).

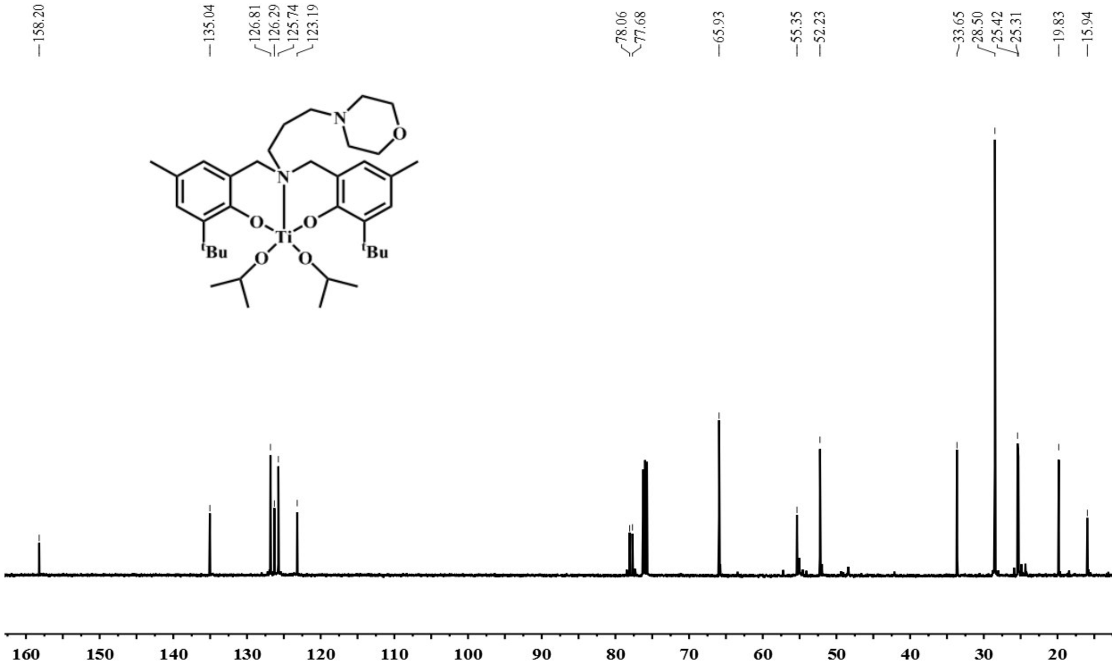

Figure S20 The ^{13}C NMR spectrum of complex **3** ($CDCl_3$, 125MHz).

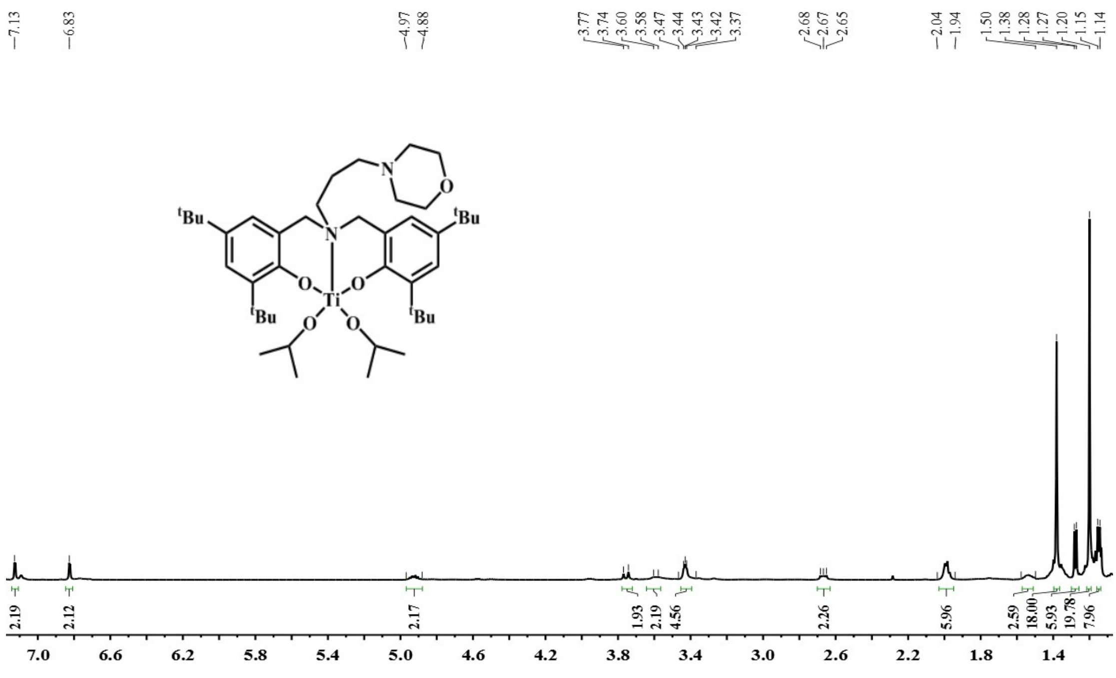

Figure S21 The ^{1}H NMR spectrum of complex **4** ($CDCl_3$, 500MHz).

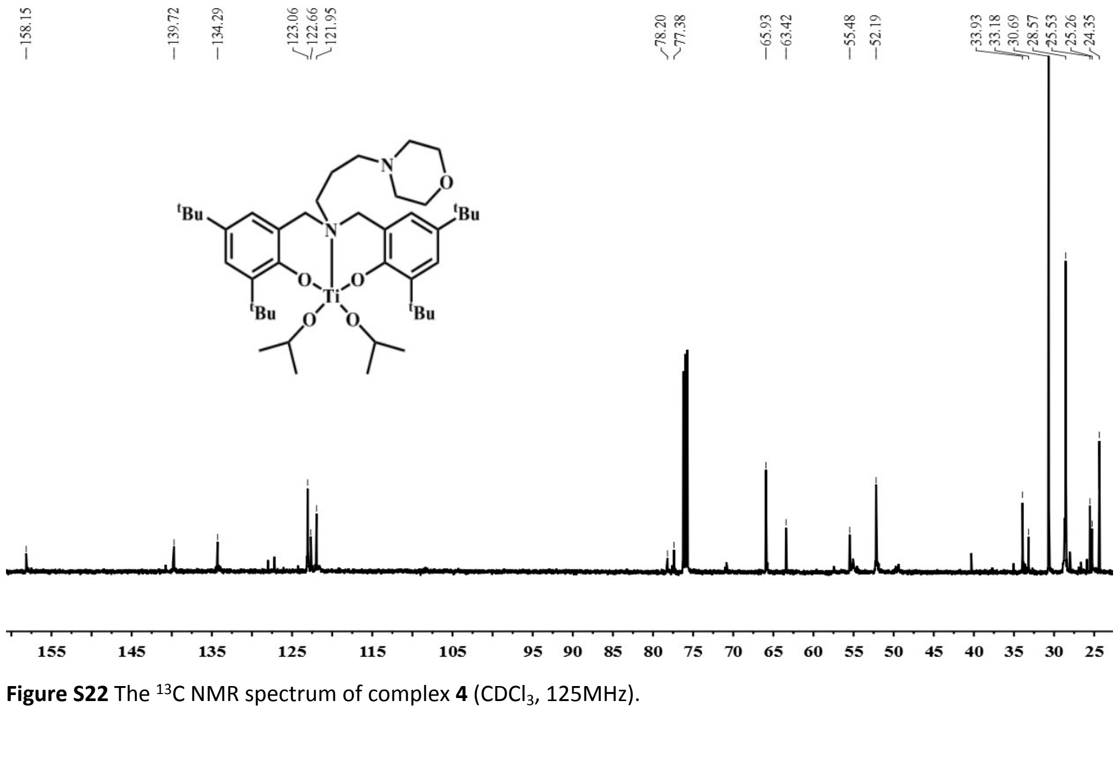

Figure S22 The ^{13}C NMR spectrum of complex **4** ($CDCl_3$, 125MHz).